

From the depletion attraction to the bridging attraction: The effect of solvent molecules on the effective colloidal interactions

Jie Chen, Steven R. Kline, and Yun Liu

Citation: *The Journal of Chemical Physics* **142**, 084904 (2015); doi: 10.1063/1.4913197

View online: <http://dx.doi.org/10.1063/1.4913197>

View Table of Contents: <http://scitation.aip.org/content/aip/journal/jcp/142/8?ver=pdfcov>

Published by the [AIP Publishing](#)

Articles you may be interested in

Erratum: "From the depletion attraction to the bridging attraction: The effect of solvent molecules on the effective colloidal interaction" [*J. Chem. Phys.* **142**, 084904 (2015)]

J. Chem. Phys. **142**, 149901 (2015); 10.1063/1.4917547

Range effect on percolation threshold and structural properties for short-range attractive spheres

J. Chem. Phys. **142**, 034504 (2015); 10.1063/1.4906084

The dynamical crossover in attractive colloidal systems

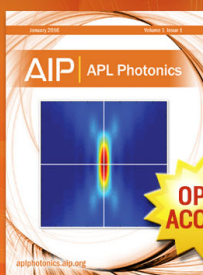
J. Chem. Phys. **139**, 214502 (2013); 10.1063/1.4833595

Polymer depletion-driven cluster aggregation and initial phase separation in charged nanosized colloids

J. Chem. Phys. **130**, 204905 (2009); 10.1063/1.3141984

Rheology of transient colloidal gels by Brownian dynamics computer simulation

J. Rheol. **43**, 219 (1999); 10.1122/1.550984



Launching in 2016!

The future of applied photonics research is here

**OPEN
ACCESS**

AIP | APL
Photonics

From the depletion attraction to the bridging attraction: The effect of solvent molecules on the effective colloidal interactions

Jie Chen,^{1,2} Steven R. Kline,² and Yun Liu^{2,3,a)}

¹*Department of Engineering Physics, Tsinghua University, Beijing, China*

²*Center for Neutron Research, National Institute of Standards and Technology, Gaithersburg, Maryland 20899, USA*

³*Department of Chemical and Biomolecular Engineering, University of Delaware, Newark, Delaware 19716, USA*

(Received 16 December 2014; accepted 9 February 2015; published online 27 February 2015)

Depletion attraction induced by non-adsorbing polymers or small particles in colloidal solutions has been widely used as a model colloidal interaction to understand aggregation behavior and phase diagrams, such as glass transitions and gelation. However, much less attention has been paid to study the effective colloidal interaction when small particles/molecules can be reversibly attracted to large colloidal particles. At the strong attraction limit, small particles can introduce bridging attraction as it can simultaneously attach to neighbouring large colloidal particles. We use Baxter's multi-component method for sticky hard sphere systems with the Percus-Yevick approximation to study the bridging attraction and its consequence to phase diagrams, which are controlled by the concentration of small particles and their interaction with large particles. When the concentration of small particles is very low, the bridging attraction strength increases very fast with the increase of small particle concentration. The attraction strength eventually reaches a maximum bridging attraction (MBA). Adding more small particles after the MBA concentration keeps decreasing the attraction strength until reaching a concentration above which the net effect of small particles only introduces an effective repulsion between large colloidal particles. These behaviors are qualitatively different from the concentration dependence of the depletion attraction on small particles and make phase diagrams very rich for bridging attraction systems. We calculate the spinodal and binodal regions, the percolation lines, the MBA lines, and the equivalent hard sphere interaction line for bridging attraction systems and have proposed a simple analytic solution to calculate the effective attraction strength using the concentrations of large and small particles. Our theoretical results are found to be consistent with experimental results reported recently. © 2015 AIP Publishing LLC. [<http://dx.doi.org/10.1063/1.4913197>]

I. INTRODUCTION

Colloidal systems are very important for many materials in our daily life, such as paint, food, soft armour,^{1,2} detergents, microemulsions,³ therapeutical drugs,⁴ and biological systems.^{5,6} A clear understanding of the effective interaction among colloidal particles is the key to control and optimize the performance of materials and their responses in different applications. One common approach is to determine an effective interaction between colloidal particles by treating all small molecules in solvent as continuous medium, which allows us to focus on the structure and dynamics of only large colloidal particles.⁷ The effect of all solvent molecules including coions and counterions is all considered implicitly in these effective interactions. Hence, effective interactions between large colloidal particles are tunable by changing the properties of small molecules. It is this tunability of effective interactions that lends us the power of controlling the properties of colloidal systems. However, even with this simplification, the understanding of colloidal systems is still very challenging despite tremendous progress.

Model colloidal systems with well-characterized interactions have been developed and investigated. Arguably, the simplest system is spherical colloidal particles with only hard sphere (HS) interaction, i.e., particles cannot overlap in space. Many theoretical and experimental works have been already devoted to study HS systems.^{8–11} The complexity of the phase behavior for a system quickly increases even by adding just one more feature, such as a short-ranged square well attraction (SW) in addition to the HS interaction (SWHS). Systems with SWHS potentials show many interesting features.^{12–17}

One of the most studied experimental SWHS systems is the PMMA colloidal system in organic solvents with added non-adsorbing polymers, such as polystyrene.^{15,18,19} Due to the osmotic pressure of added polymers in solvent, a depletion attraction is generated between large PMMA colloidal particles. This mechanism was first pointed out by Asakura and Oosawa.^{20,21} When the inter-distance of colloidal particles is smaller than the characteristic size of small particles, such as the radius of gyration of polymers, the exclusion of the non-adsorbed small particles results in a concentration gradient between the gap regions of the big particles and bulk solution. This concentration gradient pushes big particles close to each other, and generate an effective attraction,^{21,22} as schematically

^{a)} Author to whom correspondence should be addressed. Electronic addresses: yunliu@nist.gov or yunliu@udel.edu

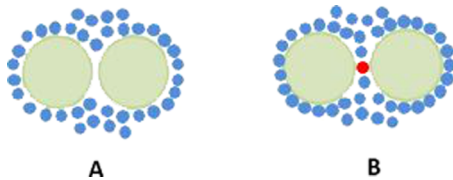


FIG. 1. Schematic figures for depletion attraction (a) and bridge attraction (b). For depletion attraction, the big particles become closer to each other because of the excluded volume effect of the small particles; for bridge attraction, one side of a small particle may be stuck to a big particle and the other side may be stuck to another one to “bridge” the big particles. To make the bridge effect clear, the “bridging” particle is shown in red.

shown in Fig. 1(a). The range of interaction can be controlled by the radius of gyration of added polymers. Systems with depletion attraction have been very successfully used to study phase behavior of SWHS systems in the past few decades.^{23–29}

In addition to introducing SW attraction using the depletion attraction, it can be also introduced by the bridging attraction. Here, unlike the case of the depletion attraction where there is no attraction between small molecules and large colloidal molecules, small molecules can be physically attracted to the surface of large colloidal particles and serve as a bridge linking two or more large colloidal particles together (see a schematic picture in Fig. 1(b)). Though some systems related with the bridging attractions have been discussed,^{30–32} the effect of bridging attractions on colloidal systems, in general, received much less attention compared to depletion attraction cases. This is partially due to the fact that there were not many good model systems. There is a great need to study this type of systems as bridging attractions potentially play important roles for many systems such as oppositely charged colloidal particles and protein solutions with different counterions.^{33–35}

Recently, Zhao *et al.* showed that by adding small particles made of Poly N-isopropyl acrylamide (PNIPAM) into large polystyrene particle solutions, PNIPAM colloidal particles can reversibly attach to the surface of polystyrene particles and introduce a bridging attraction between large particles. The system changes from a liquid to a solid-like gel by adding a very small amount of PNIPAM particles. When further adding PNIPAM particles, the system becomes liquid again. And when more PNIPAM particles are added, it becomes a solid-like gel.¹

Theoretically speaking, the difference between the depletion and bridging attraction systems lies in the difference of the interaction between small particles and large particles. Here, small particles are treated as parts of solvent molecules. If there is no attraction between small and large particles, the osmotic pressure of small particles can introduce an effective depletion attraction. When there is a strong attraction between small and large particles, an effective bridging attraction is generated. By varying the attraction strength between small and large particles, the two types of systems can be considered two extreme cases of the same type of binary colloidal systems. However, unlike the cases of the depletion attraction, there are fewer works devoted to the theoretical study of systems interacting with bridging attractions.

In this paper, we calculate phase diagrams of systems with bridging attractions by considering binary hard sphere systems

with asymmetric sizes using the multicomponent theory for sticky hard sphere (SHS) systems developed by Baxter in the 1960's.^{36,37} The size ratio between the large and small particles in our systems is chosen to be consistent with recent experimental results reported by Zhao *et al.*¹ in order to compare the calculated results with experimental values. There are only HS interactions between particles with the same size. By varying the attraction strength from zero to very large values between small and large particles, this binary particle system can change from a depletion attraction system to a bridging attraction system.

Binary SHS systems have been investigated before.^{38–48} However, we focus here on understanding the change of the effective bridging attraction and phase diagrams with different concentrations of small and large particles. As far as we know, these issues have not been addressed systematically before despite a few early studies.^{45–48} We investigate the spinodal and binodal transitions, percolation lines, and other interesting properties for bridging attraction systems. An analytical solution is developed to calculate the effective interaction between large colloidal particles. Our results are compared with the experimental phase diagram reported by Zhao *et al.*¹ We demonstrate here that binary SHS systems can successfully explain most experimental observations reported by Zhao *et al.* Some of our results nearly agree with the experimental observations quantitatively.

II. THEORIES AND METHODS

The analytic solution of the Ornstein-Zernike (OZ) equation for a one component system interacting with SHS interactions was first developed by Baxter using the Percus-Yevick (PY) closure.^{36,37} Later, using the “Q method,” he further developed theories for multicomponent systems with SHS interactions.⁴⁹ Since then, numerous works using his methods have been devoted to study the properties and phase diagrams of SHS systems.^{39,50–59} These methods have been shown to work reasonably well.^{60–63} But it should be noted that the PY approximation is lacking thermodynamic consistency. Its limits and problems have been discussed in Refs. 64 and 65.

The pair potential of a multi-component SHS system between components i and j can be described as

$$\beta U_{ij} = \begin{cases} \infty, & r < \sigma_{ij}, \\ \ln[12\tau_{ij} \frac{(d_{ij} - \sigma_{ij})}{d_{ij}}], & \sigma_{ij} < r < d_{ij}, \\ 0, & d_{ij} < r, \end{cases} \quad (1)$$

where $\beta = 1/(kT)$, k is the Boltzmann constant, and T is the absolute temperature. σ_i is the diameter of component i . $\sigma_{ij} = (\sigma_i + \sigma_j)/2$. $d_{ij} - \sigma_{ij}$ is the attraction range between components i and j . In the limiting case of SHS interaction, d_{ij} is infinitesimally close to σ_{ij} . τ_{ij} is a parameter related to the strength of the attraction between different components and is commonly called the stickiness parameter. It can be considered as an effective “temperature,” i.e., smaller τ means stronger attraction. When τ approaches infinity, there is no attraction between particles, and the interaction becomes hard sphere interaction.

In Appendix A, we have summarized all the equations needed to calculate the partial structure factors for an N-component system. At the SHS limit, d_i is the same as σ_i . The most important step of this method is to solve $N(N+1)/2$ polynomial equations (A2) for the elements of matrix Q (A1), which has an algebraical relation with structure factors (A3).

In this paper, we focus on two-component systems ($N=2$), where the size ratio between small and large particles is defined as $x = d_S/d_L$. There are only hard sphere interactions among particles with the same size, i.e., $\tau_{SS} = \tau_{LL} = \infty$. τ_{SL} , the stickiness parameter between small and large particles, is varied to have different attraction strengths between small and large particles. Because the size ratio is small, the small particles can be considered as parts of solvent molecules, such as polystyrene in PMMA colloidal solutions (depletion attraction case) and PNIPAM polymers in large PS solutions (bridging attraction case), which are added to solutions to change the effective interaction between large colloidal particles. For a depletion attraction, τ_{SL} is very large. For the bridging attraction case, τ_{SL} is very small. In this paper, we focus on bridging attraction cases. The partial structure factors, $S_{LL}(q)$, $S_{SL}(q)$, and $S_{SS}(q)$, can be calculated analytically. Since our focus is on large colloidal particles, $S_{LL}(q)$ will be used to help identify phase diagrams of large colloidal particles.

A. Calculation of spinodal regions

It has been demonstrated that at relatively dilute colloidal concentrations, gelation is related to the arrested spinodal decomposition.¹⁹ Hence, the understanding of the spinodal decomposition line (SDL) is very useful to understand the gelation of bridging attraction systems. The SDL can be calculated analytically in binary SHS systems. The details are given in Appendix A 2. For a given attraction strength τ_{SL} between big and small particles and size ratio x , the SDL in $\phi_S - \phi_L$ plane is

$$3 + \frac{\sqrt{(3 + \frac{1-\phi}{\phi_S})(3 + \frac{1-\phi}{\phi_L})}}{\frac{(1+x)^2}{4x}(1-\phi)} = \frac{(1+x)(1-\phi) + 3(\phi_S + x\phi_L)}{\frac{1-\phi}{4x}(\phi_S + x\phi_L)(1+x)^2 + (1+x)(\phi_S + x\phi_L)^2\tau_{SL}}, \quad (2)$$

where ϕ_S and ϕ_L are the volume fractions of small and large particles, respectively, and $\phi = \phi_S + \phi_L$. This is equivalent to Eq. (A8), the points on the SDL correspond to the divergence of $S_{LL}(q=0)$.³⁶

B. Mapping binary systems to one-component SHS systems

Because our focus is on phase diagrams of large colloidal particles, we can calculate an equivalent one component SHS system whose phase diagram is the same as that of large particles in our binary colloidal systems. There are three parameters in one-component SHS system: the particle diameter (σ^{eff} , also d^{eff} for SHS), volume fraction (ϕ^{eff}), and the stickiness parameter (τ^{eff}). Here, the superscript “eff” means the param-

eters of the one-component system determined by the effective potential. Once these three parameters are known, the phase behavior can be determined for this equivalent one component SHS system.

We first need to estimate d^{eff} . It is important to note that d^{eff} is not necessarily the same as d_L . It is the closest distance that two large particles can approach each other. When τ_{SL} is small, small particles can strongly bind to the surface of large particles. The equivalent excluded volume of large particle has to include the volume of small particle on the surface. As a result, d^{eff} is larger than d_L . It is not easy to estimate d^{eff} for a general case. But at the limit of small τ_{SL} , which is the case in this paper, d^{eff} can be calculated analytically using the size information of two component systems as

$$\frac{d_L^{eff}}{d_L} = \frac{2}{3} \left(1 + x + \frac{1}{2+x} \right). \quad (3)$$

The details of the calculation is given in the Appendix (Appendix B).

Once d^{eff} is known, the effective volume fraction, ϕ^{eff} , can be estimated by equating the number density of large colloidal particles in the binary system and the equivalent one-component system through the relation $\phi^{eff}/\phi_L = (d^{eff}/d)^3$.

τ^{eff} determines the effective interaction potential between large colloidal particles and is a complex function of parameters of two component systems, i.e., $\tau^{eff} = f(x, \phi_S, \phi_L, \tau_{SL})$. In order to evaluate τ^{eff} , we require that the value of structure factor at $q=0$ is the same for $S_{LL}(0)$ and $S^{eff}(0)$, where $S^{eff}(0)$ is calculated using one component theory using d^{eff} , ϕ^{eff} , and τ^{eff} . As shown in Appendix B, the effective stickiness parameter τ^{eff} can then be calculated analytically as

$$\tau_L^{eff} = \left[\frac{(1-\phi_L^{eff})^2}{36} S_{LL}(0) + \frac{4\phi_L^{eff}-1}{18} \sqrt{S_{LL}(0)} - \frac{14(\phi_L^{eff})^2 - 4\phi_L^{eff} - 1}{36(1-\phi_L^{eff})^2} \right] / \left[\frac{2\phi_L^{eff} + 1}{3(1-\phi_L^{eff})} - \frac{1-\phi_L^{eff}}{3} \sqrt{S_{LL}(0)} \right]. \quad (4)$$

Even though we only require $S^{eff}(0) = S_{LL}(0)$, we find that $S^{eff}(q)$ is almost identical to $S_{LL}(q)$ for all of the q range for most cases studied in this paper, which means the proposed mapping method from a two-component system to an equivalent one-component system is valid. We also emphasize that all calculated parameters have analytical solutions, which makes this mapping method very efficient.

III. RESULTS AND DISCUSSIONS

Without losing generality, we have chosen the size ratio, x , to be 0.1444, consistent with the experimental value reported by Zhao *et al.*^{1,66} The advantage is that we then can compare our theoretical results to the experimental ones to offer physical interpretations of experimental systems. The studied volume fractions for both ϕ_S and ϕ_L range from about 0% to 40%, which is compatible with the concentration range investigated by experiments.^{1,66} Our methods can be extended to many other cases with different particle size ratios.

A. Difference between the depletion attraction and the bridging attraction

As aforementioned, by varying τ_{SL} , this two component system model can change from a depletion attraction system to a bridging attraction system. Therefore, it is interesting to compare the structures of these two cases by calculating $S_{LL}(q)$. For the depletion attraction case, this can be approached by setting the parameter τ_{SL} to a very large value. To compare the two different mechanisms, τ_{SL} has been set to 10 000 and 0.02 for the depletion and bridging attraction cases, respectively.

Fig. 2 shows the change of $S_{LL}(q)$ by varying volume fractions of small particles. (a) and (b) are for the depletion attraction cases, while (c) and (d) are for the bridging attraction. ϕ_L is chosen to be 4% as an example. However, the general observation studied here can also be extended to other volume fractions.

For a given ϕ_L , the intensity of $S_{LL}(0)$ is related to the strength of the effective attraction between large particles. Larger values of $S_{LL}(0)$ mean stronger attractions. As shown in Figs. 2(a) and 2(b), when increasing the volume fraction of small particles (ϕ_S), $S_{LL}(0)$ monotonically increases, indicating that the addition of small particles increases the strength of the depletion attraction. Associated with the increase of depletion attraction, the first peak position shifts slowly to larger q values indicating that large particles aggregate so that the inter-particle distance becomes smaller. For binary hard sphere systems, even though a more accurate estimation of an effective depletion attraction due to small particles can be achieved by constructing an effective Hamiltonian proposed by Dijkstra and co-workers,⁶⁷ the current method can still catch the qualitative trend.¹⁶

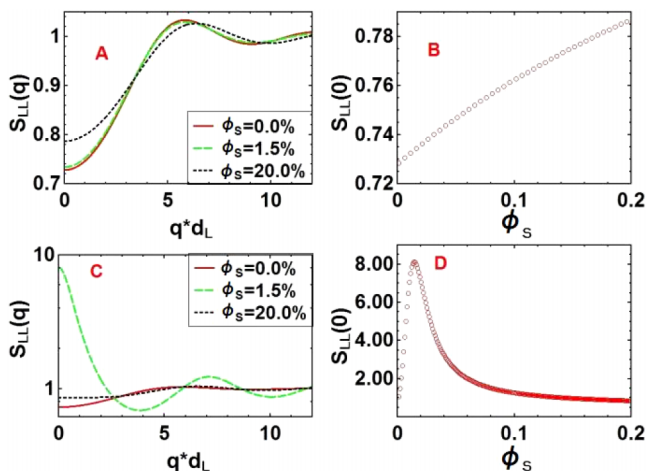


FIG. 2. Comparison between depletion and bridge interactions. For all the figures, the size ratio of small to large particle is $x = 0.1444$ and the volume fraction of large particles is 4%. (a) and (b) are with the same attraction strength ($\tau_{SL} = 10\,000$, introducing depletion attraction) between small and large particles, while it is 0.02 (introducing bridging attraction) for (c) and (d). (a) and (c) show the partial structure factors for large particles with different volume fractions of small particles, as told in the figures, (b) and (d) show the values of partial structure factors at $q = 0$ with increasing small particles' volume fraction. To make the difference clear, y axis of (c) is shown in logarithmic scale.

However, this concentration dependence is dramatically different in the bridging attraction case as shown in Figs. 2(c) and 2(d). Unlike the previous case where the small change of ϕ_S at the beginning has a very minor effect to $S_{LL}(q)$, $S_{LL}(q)$ in (C) shows a large low- q upturn even at $\phi_S = 1.5\%$. The intensity of $S_{LL}(0)$ in Fig. 2(d) first increases and reaches a peak before it finally slowly decays. This shows that the increase of ϕ_S first increases the effective attraction favoring the particle aggregation. However, when there are enough small particles, the further increase of ϕ_S actually stabilizes the large colloidal particles as the effective attraction becomes smaller. This is because that when more and more small particles stick to the surface of large particles, the “coated” large particles will not have strong attraction between them any more since there is no attraction between the “shells” of small particles. As a result, the large particles are stabilized by the addition of small particles. Therefore, this can be a different way of stabilizing large colloidal particles by introducing small molecules that can stick to the surface of large colloidal particles.

The inter particle distance between large particles is consistent with the change of attractions in both depletion and bridge attraction cases. Assuming that the position of first order diffraction peak is q_0 , the inter-particle distance of large colloidal particles can be approximately estimated as $2\pi/q_0$ as shown in Fig. 3. The open circles and stars are for the depletion and bridging attraction cases, respectively. When increasing small particle concentrations, the inter-particle distance for the depletion attraction case decreases slowly as more attraction favors closer packing of large particles. However, for the bridging attraction case, the addition of small colloidal particles first decrease the inter-particle distance dramatically favoring aggregation. Once ϕ_S reaches certain value, the inter-particle distance increases as small particles can coat the surface of large particles. When ϕ_S is large enough, the small particles will not introduce attraction effect. Instead, it generates an effective repulsion between large colloidal particles. Because of the difference of the depletion and bridging attraction, it has different consequences to their phase diagrams that can partially explain the phase behavior of experimental results reported by Zhao *et al.*^{1,66}

B. Phase diagrams of large colloidal particles

As the spinodal decomposition line (SDL) is intrinsically linked to the gel formation at low concentrations, it is very

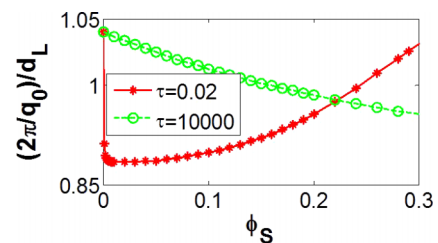


FIG. 3. The inter-particle distance normalized to the diameter of large particles versus the volume fraction of small particles for depletion attraction (green circles with dashed line) and bridge attraction (red stars with solid line). The volume fraction of large particles is 4% and the diameter of small and large particles is the same with Fig. 7.

interesting to calculate SDL in our systems. As mentioned before, in order to compare our calculations to the experimental results, we have fixed the size ratio x to be 0.1444.

SDL is very sensitive to the value of τ_{SL} . Different SDLs calculated using Eq. (2) are shown in Fig. 4 for different values of τ_{SL} . The volume fraction of large and small particles are chosen to be the horizontal and vertical axes, respectively, as the recent phase diagrams of experimental results of bridging attraction are reported in this way. The spinodal regions form isolated islands encompassed by the SDL. Within the area delimited by the SDL, systems become unstable. The areas for these spinodal islands increase by decreasing τ_{SL} . It seems that the size of area saturates at $\tau_{SL} = 0.001$. Decreasing τ_{SL} further does not change the shape and area of the island too much. When increasing τ_{SL} , the spinodal region shrinks. If $\tau_{SL} \approx 0.017$, the spinodal island shrinks to almost a point (the red star in Fig. 4), which we define as “ $\tau_{critical}$.” For $\tau_{SL} > \tau_{critical}$, systems do not show any spinodal decomposition for any volume fraction compositions. Since the binodal transition line and spinodal transition line collapse to the same point at $\tau_{SL} = \tau_{critical}$, there is no binodal phase transition either when $\tau_{SL} > \tau_{critical}$. Hence, systems are always stable as there are no phase separations happening when the attraction is small enough, i.e., τ_{SL} is large enough. Note that when τ_{SL} is too large, i.e., the attraction between small and large particles is very weak, the depletion attraction dominates and can result in a phase separation of large colloidal particles at large ϕ_S . The limiting case for weak attraction is a binary HS system that shows interesting liquid-liquid and liquid-solid transitions as discussed by Dijkstra and co-workers.⁶⁷ It is important to also point out that $\tau_{critical}$ is very sensitive to particle size ratio. When x become smaller, $\tau_{critical}$ increases. Therefore, when small particle becomes smaller, weaker attraction between small and large particles is needed to introduce phase transitions of binary colloidal systems.

When τ_{SL} is small enough (strong bridging attraction case), the formed spinodal region always appears where ϕ_S is small as demonstrated in Fig. 4. If there are no small particles, samples are stable because there is only HS interaction between

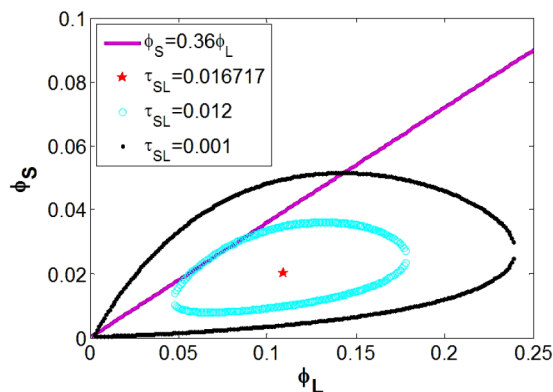


FIG. 4. Spinodal decomposition lines for systems with different attraction strengths between small and big particles (see the legend). The size ratio is $x = 0.1444$, the linear relation of the purple solid line is from Ref. 1, which means the volume fraction of small particles need to cover the surface of big particles. The star represents the critical stickiness parameter above which the system will never show spinodal decomposition phenomenon.

large particles. By increasing ϕ_S to even a very small value, the system immediately becomes unstable by entering the spinodal region. With more small particles, it will eventually move out of the spinodal region. Lu *et al.* has demonstrated that at low particle concentration, the gelation transition is driven by spinodal decomposition.¹⁹ We can use the SDLs to roughly estimate the gelation transitions in bridging attraction systems. Therefore, we would expect that adding small particles can cause gel formation when the system starts entering the spinodal island. Further adding small particles, the system should move out of the spinodal region and become liquid again. This observation is consistent with the experiment reported by Zhao *et al.*^{1,66}

In order to use our theories to better understand the experimental system,^{1,66} we attempted to estimate τ_{SL} between small and large particles. The purple solid line shown in Fig. 4 is the saturation line from Zhao’s paper.¹ According to their interpretation, this straight line represents the number of small particles needed to fully cover the surface of big particles. It is difficult for our theory to predict the coverage of small particles on large particles as small particles on large particle surface is always at dynamic equilibrium due to the exchange of particles on surfaces with ones in solvent. During the experiment, they observed the large particle aggregation using a microscope at very small ϕ_L . They reported that their systems become stable (have fewer aggregates) again when ϕ_S reaches the straight solid line. This indicates that this straight line may be close to the transition line from a gel state to a liquid state. We, hence, estimated τ_{SL} by allowing the SDL to overlap as much as possible with the saturation line. The estimated value is $\tau_{SL} = 0.012$ whose spinodal line is shown as cyan circles in Fig. 4. This is a very rough estimation of τ_{SL} . But interestingly, this estimated result can explain many of their observations quantitatively as shown later. The following calculation in the paper will assume $\tau_{SL} = 0.012$ and $x = 0.1444$ unless explicitly stated otherwise.

Once the size ratio, x , and the attraction strength, τ_{SL} , are determined, we can calculate all partial structure factor, from which we can obtain much useful information. We first focus on $S_{LL}(0)$. As we noted already, large $S_{LL}(0)$ means large attraction strength (small τ^{eff}) between large colloidal particles at a given ϕ_L . Fig. 5 shows the change of $S_{LL}(0)$ as a function of ϕ_S at a given ϕ_L .

At $\phi_L = 0.1\%$, the increase of ϕ_S first increases $S_{LL}(0)$ very sharply and reaches a maximum, indicating that the effective attraction strength between large particles reaches maximum at about $\phi_S = 0.6\%$. This concentration is termed as the maximum bridge attraction (MBA) concentration. By further increasing ϕ_S , $S_{LL}(0)$ decreases slowly. At $\phi_S = 33.0\%$, $S_{LL}(0)$ is the same as that at $\phi_S = 0$. This value of ϕ_S is termed as equivalent hard sphere (EHS) point as at this EHS volume fraction, the osmotic compressibility of the binary systems is identical to that of a HS system at the same volume fraction. A structure factor comparison of the two-component SHS system at the EHS point and one-component HS system with the same volume fraction of big particles for the four points in Fig. 5 is shown in the supplementary material.⁶⁸

At this ϕ_L (0.1%), $S_{LL}(0)$ remains finite in a wide range of ϕ_S . Therefore, there is no spinodal region. At $\phi_L = 10.0\%$, $S_{LL}(0)$ quickly diverges as the increase of ϕ_S . There is a gap

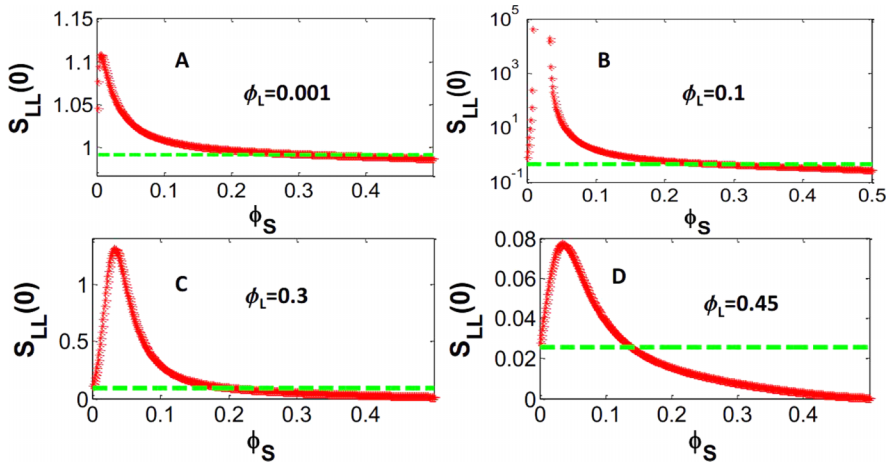


FIG. 5. Partial structure factor of large particles at $q = 0$ with different volume fractions as shown in the figures. Green line means the structure factor value at $q = 0$ for pure hard sphere system with volume fraction of corresponding ϕ_L^{eff} .

for $S_{LL}(0)$ from $\phi_S = 0.9\%$ to $\phi_S = 3.4\%$ as the calculated value of $S_{LL}(0)$ is not physically meaningful in the unstable regions. When $\phi_S > 3.4\%$, $S_{LL}(0)$ begins to decrease and eventually reaches the EHS concentration. For $\phi_L = 30.0\%$ and 40.0% , the change of $S_{LL}(0)$ shows a trend similar to that at $\phi_L = 0.1\%$. There are no spinodal transition regions for these two cases.

We have calculated the lines for SDL (cyan open circles), MBA (red stars), and EHS (green open circles), which are plotted in Fig. 6. Clearly, MBA and EHS concentrations vary at different ϕ_L . Because the EHS line lies at larger concentrations, it is shown in the inset of Fig. 6. The EHS line is fitted to a linear function as $\phi_S = -0.4245\phi_L + 0.3311$. We will compare this phase diagram with the experimental results later in this paper. (Points A and B indicated in the figure are the conditions for experimental data.)

C. Validation of the mapping method

As mentioned earlier in Sec. II B, we can benefit from the extensive investigations of one component SHS systems by mapping out this two component system to an equivalent one component SHS system that has been carefully studied both theoretically and experimentally for many decades.^{36,37,49–52} Since we focus on phase behavior of large colloidal particles, and the size ratio, x , is small, we can attribute the effect of the solvent molecule (small particles) to the effective attraction

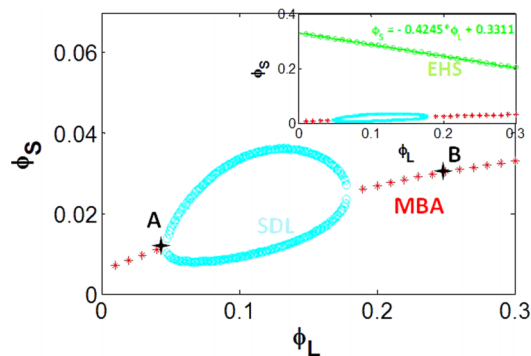


FIG. 6. State diagram for our system. The inset is all the information from Fig. 5 for the volume fraction range interested and the main panel is the local scale for SDL and MBA. The line in the inset is the linear fitting of the EHS points.

between large colloidal particles, which is sensitive to the properties of small particles, such as size and concentration. Once having this effective potential, theories for one-component SHS systems can be applied to understand the phase diagrams of large colloidal particles in our two component systems. As $S(q)$ is a measure of inter-particle structure, all thermodynamic quantities, such as pressure, energy, can be calculated using $S(q)$. The calculation of the effective potential of a one-component system finds a correct set of parameters (τ^{eff} , ϕ^{eff} , and d^{eff}) to reproduce $S_{LL}(q)$.

The details of this mapping method are given in Sec. II B. Here, we would like to compare the structure factor ($S(q)$) between two component systems and ones calculated from this mapping method. Fig. 7 shows the structure factor comparison of this method for four cases. These four cases are chosen to

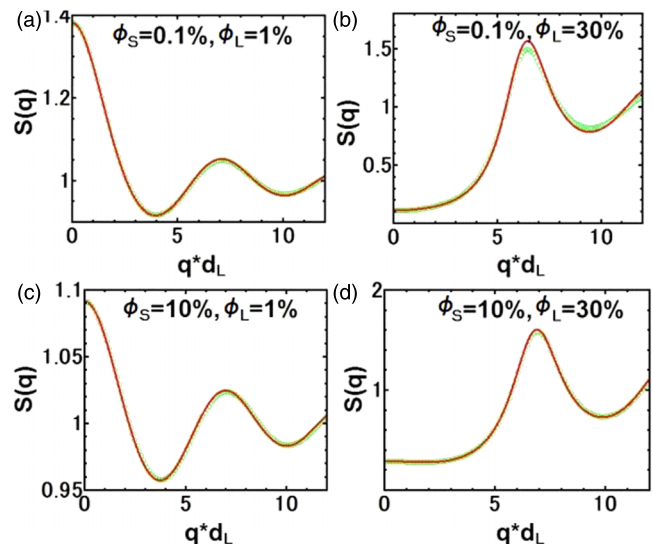


FIG. 7. The structure factor comparison of binary hard sphere system (green open circles) with the equivalent pure hard sphere system (red solid line). In the binary systems of both figures, the parameter for attraction between small and large particles is $\tau_{SL} = 0.012$, the diameters of small and large particles is 260 \AA and 1800 \AA , respectively, and the volume fractions are on the plots. The corresponding equivalent pure SHS system is mapped by the method described in the context, the effective “diameter” is $d^{\text{eff}} = 1932.8 \text{ \AA}$, and the others are (a) $\tau^{\text{eff}} = 0.0686$, $\phi^{\text{eff}} = 0.0124$; (b) $\tau^{\text{eff}} = 0.7472$, $\phi^{\text{eff}} = 0.3715$; (c) $\tau^{\text{eff}} = 0.1335$, $\phi^{\text{eff}} = 0.0124$; (d) $\tau^{\text{eff}} = 0.2378$, $\phi^{\text{eff}} = 0.3715$. Recall it that d^{eff} is the effective inter-particle distance rather than diameter. Here x axis is scaled by the diameter of large particles (1800 \AA) to make it more general.

cover a wide range of regions of the phase diagram in Fig. 6. The solid lines are the calculated $S^{eff}(q)$ of one component SHS system and the green circles are $S_{LL}(Q)$ from two component systems. The agreements are excellent in our cases. We would like to emphasize again that the calculations in our proposed method are all analytical. The solid lines are not fits, but simply calculated curves from our method without fitting parameters. The structure factor over the whole q range can be almost exactly reproduced. Of course, once the experimental conditions have reached the EHS line or beyond, our proposed method will not work. In the supplementary material,⁶⁸ we show the region in the phase diagram where our proposed method works best.

Once we have τ^{eff} , ϕ^{eff} , and d^{eff} , we are able to use the results obtained from one component SHS to determine the phase diagram of large particles in our two-component systems.

D. Percolation threshold and binodal lines

First, we would like to calculate the percolation as this an important property of a SHS system that has been studied extensively.⁵²

The percolation lines of one component SHS systems have been calculated analytically by Glandt with PY approximation to be⁵⁵

$$\tau^{eff} = \frac{12\phi^{eff2} - 2\phi^{eff} + 1}{12(1 - \phi^{eff})^2}. \quad (5)$$

Here, percolation is defined as the point at which there is at least a system-spanning cluster.

Equation (4) is used to calculate the effective stickiness parameter, τ^{eff} , from a two component system. Given ϕ_L and ϕ_S , we obtain τ^{eff} and ϕ^{eff} and use Eq. (5) to estimate the percolation lines. The calculated percolation region for the two component systems is sandwiched by two lines (filled blue circles) as shown in Fig. 8. When adding small particles, the system is able to percolate at very small ϕ_S and then exits the percolated region when there is an excess of small particles.

We did not calculate the percolation line at small volume fraction of large particles ($\phi_L < 7.7\%$) even though this can be done by following Eq. (5). At small ϕ_L , the structure factor

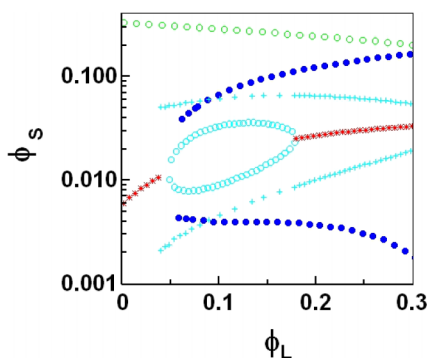


FIG. 8. The phase diagram for binary system with size ratio $x = 0.1444$ and inverse stickiness parameter $\tau_{SL} = 0.012$. The symbols are green circles for EHS, blue filled circles for percolation, cyan crosses for binodal line, cyan circles for SDL and red stars for MBA. Logarithmic scale is used for y axis to show more details, and a linear scale version is shown in supplementary material.⁶⁸

calculated from Baxter's method for one component system is not very accurate when the system is close to the instability line, which is obtained by finding the unphysical solutions in the Baxter's method, and is commonly assigned as the spinodal line. (It is well known that at low concentration, $S(q)$ calculated using Baxter's method will not diverge at the estimated instability line.³⁶) However, since Baxter's method works well at large ϕ_L ,^{52,61} we would expect that the percolation lines at larger ϕ_L is quantitatively more accurate. We also would like to point out that this issue only affects the percolation and binodal line estimation using one component theories in our works. There is no problem calculating the instability lines (spinodal decomposition lines) using Baxter's multi-component theory.

Note that the percolation lines of two component systems can be also directly calculated using multi-component theory proposed by Baxter.⁴⁵⁻⁴⁸ The results have been shown in the supplementary material (Fig. S3),⁶⁸ where the system spanning clusters include both small and large particles. Since we focus on only large particles here, the calculated percolation region is only a subset of the percolation region directly calculated for two-component systems.

Miller and Frenkel⁵² have also calculated the binodal transition line for one-component SHS system through grand canonical MC simulation. By mapping two component systems to the equivalent one-component SHS system, we are able to identify the binodal lines of large colloidal particles in our two component systems. The results are shown in Fig. 8 as cyan pluses (+). The regions between the two binodal lines are two phase regions. We do not have results for $\phi_L < 4\%$ as Miller and Frenkel's simulation⁵² did not simulate the cases for $\phi_L < 4.0\%$.

E. Comparison with the experimental results

In their experiments, Zhao *et al.* observed liquid-gel-liquid phase transitions by progressively adding small particles (PNIPAM) for some volume fractions of large particles (PS).¹ These liquid-gel-liquid phase transitions can be qualitatively explained by the isolated spinodal regions at moderate volume fraction range for large particles. Also, it has been found that their experimental systems cannot form gel when the volume fraction of large particles (polystyrene) is smaller than 5%.¹ Very interestingly, this happens to be the left boundary of the spinodal region (point A in Fig. 6). It was also reported that in a gel state at $\phi_L = 25\%$, the mechanical strength of the gel becomes strongest at ϕ_S between 2% and 5% as the storage modulus for a sample at $\phi_L = 25\%$ reaches the maximum value at this concentration range of ϕ_S .¹ Our results indicate that ϕ_S reaches the MBA concentration at about 3.0% (Point B in Fig. 6) with $\phi_L = 25\%$. Therefore, the effective attraction strength between large particles is the strongest at $\phi_S = 3.0\%$, which agrees excellently with the small particle volume fraction at which the storage modulus reaches a peak. Hence, the experimental system observed by Zhao *et al.* can be explained indeed by bridging attraction and can be modelled as a binary SHS system.

Despite the agreement with some of their experimental results, our theoretical models are still different from the experimental systems. For example, the small particles (PNIPAM

gel particles) in their experiments are relatively soft and may deform when they are attached to the surface of large particles while both small and large particles are treated as non-deformable hard spheres in our models. These differences can lead to some difference between theoretical calculations and experimental observed results.

Also, our theoretical results indicate that once moving out of the spinodal region, the effective attraction strength between large colloidal particles decreases continuously that is unlikely to introduce another gelation transition. However, experimentally, their samples can re-enter the gelation region at very large ϕ_S . The current paper focuses on the equilibrium phase diagrams while the gelation and glass transitions are related with the kinetic phase diagrams, especially at large concentrations of small and large particles. It will be interesting to calculate the kinetic phase diagrams in future works using existing theories.^{69–73}

IV. CONCLUSION

There is current interest in understanding bridging attraction systems where small molecules added to solutions can be reversibly attracted to the surface of large colloidal particles to serve as a bridge linking two large particles. Interesting phase behavior has been reported recently. This kind of model colloidal systems differs from the widely used depletion attraction systems where small particles cannot be adsorbed on the large particle surface. Therefore, it is of great interest to understand these systems theoretically.

In this paper, we have applied the multi-component SHS theory proposed by Baxter to calculate the equilibrium phase diagrams of two component SHS systems with asymmetric sizes. This model can be used to understand qualitatively the behavior for both depletion attraction and bridging attraction systems. We have focused on the bridging attraction case where the attraction between small and large particles is very strong. The equilibrium phase diagrams including spinodal region, percolation threshold, and binodal phase transition lines are calculated. By using the experimental information as the input of the theory, the calculated results are compared with experimental observations. Qualitative agreement between the theoretical results and experimental observations is found indicating that the previously observed experiment results can be explained with liquid theories of two component systems with bridging attraction.

It is well-known that many depletion attraction systems can be modelled by SHS systems. Here, we demonstrate that the bridging attraction system can be also modelled as an equivalent SHS system when the small particle concentration is below the EHS concentration. At the limit of strong attraction, we have proposed a method to analytically calculate the parameters for the equivalent one-component SHS system. Unlike the depletion attraction case where the effective attraction increases monotonically as the concentration of small particles increases, the dependence of the effective attraction on small particle concentration is highly non-trivial for bridging attraction systems. At small ϕ_S , increasing ϕ_S sharply increases the effective attraction strength between large parti-

cles. After reaching a maximum effective attraction strength, adding more small molecules decreases the attraction strength between large particles. When the concentration of small particles is larger than the EHS concentration, the small particles cannot introduce effective attraction any more between large particles. Instead, it introduces an effective repulsion between large particles. Hence, in bridging attraction systems, adding enough small particles can essentially stabilize large colloidal particles. Because of this non-monotonic dependence of the effective attraction strength between large colloidal particles on ϕ_S , it results in the formation of isolated two phase regions of large colloidal particles. Outside of these isolated regions, the bridging attraction systems are stable. For a given size ratio, there is a threshold value for the stickiness parameter between small and large particles, above which there is no phase separation observed based on our theoretical calculations. This also poses a requirement if one would like to generate a gel phase for a bridging attraction system as the gelation at low concentration is believed to be related to spinodal decomposition.

Even though through our paper, we have focused on comparing our theoretical phase diagram with recent experimental reports in neutral colloidal systems, we believe that our theoretical approaches can be also used to understand oppositely charged colloidal systems and counterion condensation in protein systems. It was recently reported that adding trivalent counterions can make BSA protein solutions turbid. By adding more counterions, the protein can become transparent again.³⁵ This observation is also qualitatively similar to what we observe in our phase diagrams. Of course, more work needs to be done in order to quantitatively explain this experimental phenomenon.

ACKNOWLEDGMENTS

This manuscript was prepared under the partial support of the cooperative Agreement No. 70NANB10H256 from NIST, U.S. Department of Commerce. The statements, findings, conclusions, and recommendations are those of authors and do not necessarily reflect the view of NIST or the U.S. Department of Commerce.

APPENDIX A: THEORIES FOR MULTI-COMPONENT SHS SYSTEMS

1. General case

The pair potential for a multi-component SHS system is shown in Eq. (1). The average SHS diameter a is defined as

$$a^3 = \sum_i x_i (\sigma_i + \Delta_i)^3.$$

Here n_i is the number density of component i and $n = \sum_i n_i$. $x_i = n_i/n$ is the number ratio.

Now, we define $d_i = (\sigma_i + \Delta_i)/a$ and $d_{ij} = (d_i + d_j)/2$. The Q matrix for Baxter's Q method is found to be^{37,39}

$$Q_{nm}(q) = \delta_{nm} + \frac{\pi a^3}{6} \sqrt{n_n n_m} \exp^{iqad_n/2} \times [-\lambda_{nm} d_m d_{nm}^2 j_0(qad_m/2)]$$

$$\begin{aligned}
& + \frac{3d_n d_m^2}{1 - \varepsilon_3} j_0(qad_m/2) \\
& + 3a_n d_m^3 \times \frac{j_1(qad_m/2)}{qad_m/2} \\
& - i \times \frac{3d_n d_m^2}{1 - \varepsilon_3} j_1(qad_m/2) \quad (A1)
\end{aligned}$$

with

$$\begin{aligned}
\tau_{nm} \lambda_{nm} = & \frac{1}{1 - \varepsilon_3} + \frac{3a\varepsilon_2}{2(1 - \varepsilon_3)^2} \times \frac{d_n d_m}{d_{nm}} \\
& - \frac{1}{2(1 - \varepsilon_3)} \times \frac{1}{d_{nm}} \times \frac{\pi}{6} a^3 \\
& \times \left[\sum_k (n_k d_{nk}^2 d_k d_m \lambda_{nk} + n_k d_{mk}^2 d_k d_n \lambda_{mk}) \right] \\
& + \frac{1}{12} \times \frac{\pi}{6} a^3 \sum_k n_k \frac{d_{mk}^2 d_{nk}^2}{d_{nm}} \lambda_{mk} \lambda_{nk}, \quad (A2)
\end{aligned}$$

$$\varepsilon_n = \frac{\pi}{6} \sum_k n_k (ad_k)^n,$$

$$X_n = \frac{\pi}{6} a^3 \sum_k n_k d_{nk}^2 d_k \lambda_{nk},$$

$$a_n = \frac{1 - X_n}{1 - \varepsilon_3} + \frac{3ad_n \varepsilon_2}{(1 - \varepsilon_3)^2},$$

$$j_0(x) = \frac{\sin x}{x}, \quad j_1(x) = \frac{\sin x - x \cos x}{x^2}.$$

To calculate the Q matrix, the key step is to solve the $N(N+1)/2$ non-linear equations for λ_{nm} as shown in Eq. (A2), where N is the number of components.

Assume $Q_{nm}(q) = Q_{nm}^r(q) + i \times Q_{nm}^i(q)$, where $Q_{nm}^r(q)$ and $Q_{nm}^i(q)$ are the real and imaginary part, respectively. Then through the direct correlation function $c(r)$, the structure factor matrix is calculated as⁷⁴

$$S(q)^{-1} = I - C(q) = Q(-q)^T Q(q). \quad (A3)$$

$C(q)$ is the Fourier transformation of $c(r)$. I is the unit matrix. The (i, j) th element of structure factor matrix, $S(q)$, is the partial structure factor between components i and j , whose inverse matrix is

$$\begin{aligned}
(S(q)^{-1})_{ij} &= \sum_k Q_{ik}^*(q) Q_{kj}(q) \\
&= \sum_k (Q_{ik}^r(q) Q_{kj}^r(q) + Q_{ik}^i(q) Q_{kj}^i(q)) \\
&+ i \sum_k (Q_{ik}^r(q) Q_{kj}^i(q) - Q_{ik}^i(q) Q_{kj}^r(q)). \quad (A4)
\end{aligned}$$

The imaginary part was found to be 0 and the structure factor to be real.

The spinodal decomposition from the compressibility equation is defined as $|Q(0)| = 0$.^{39,56} Substitute this into Eq. (A1) and apply the limit $j_0(x \rightarrow 0) = 1$, $j_1(x \rightarrow 0) = x/3$ to get

$$\begin{aligned}
Q_{nm}(0) = & \delta_{nm} + \frac{\pi a^3}{6} \sqrt{n_n n_m} \\
& \times \left[-\lambda_{nm} d_m d_{nm}^2 + \frac{3d_n d_m^2}{1 - \varepsilon_3} + a_n d_m^3 \right]. \quad (A5)
\end{aligned}$$

2. Spinodal decomposition lines

For the system studied in this article, the component number is $N = 2$ and $\tau_{SS} = \tau_{LL} = +\infty$, which makes λ_{SS} and λ_{LL} to be zero. So we solve one equation for one variable λ_{SL} from Eq. (A2) that can be expressed as

$$\lambda_{SL} = \frac{\varepsilon(1+x) + 3(\eta_S + x\eta_L)}{\frac{\varepsilon}{4x}(1+x)^2(\eta_S + x\eta_L) + (1+x)\varepsilon^2\tau_{SL}}, \quad (A6)$$

where

$$\eta_\alpha = \frac{\pi}{6} (ad_\alpha)^3 n_\alpha,$$

$$\varepsilon = 1 - \varepsilon_3 = 1 - \eta_S - \eta_L,$$

$$x = \frac{d_S}{d_L}.$$

At the SHS limit, x is the diameter ratio of small particles to large particles. η_α is volume fraction ϕ_α . The total volume fraction $\phi = \phi_S + \phi_L = \varepsilon_3$. By forcing $|Q(0)| = 0$ in Eq. (A5), we obtain

$$\lambda_{SL} = \frac{3 + \sqrt{(3 + \frac{\varepsilon}{\phi_S})(3 + \frac{\varepsilon}{\phi_L})}}{\varepsilon \frac{(1+x)^2}{4x}}. \quad (A7)$$

Equations (A6) and (A7) are two expressions for λ_{SL} at spinodal decomposition points, so the right hand side of these two equations should be equal to each other. Hence, we can obtain

$$\tau_{SL} = \frac{(1+x)[(1+x)(1-\phi) - \Delta(\phi_S + x\phi_L)]}{4x(1-\phi)(3+\Delta)}, \quad (A8)$$

where

$$\Delta = \sqrt{9 + \frac{\phi(3-2\phi)}{\phi_S \phi_L}}.$$

So with fixed attraction between small and large particles and their diameter ratio, the spinodal decomposition lines in the volume fraction plane can be calculated from Eq. (A8).

APPENDIX B: MAPPING BINARY SYSTEMS TO EQUIVALENT ONE-COMPONENT SHS SYSTEMS

We first calculate the average inter-particle distance between large particles, d^{eff} . As shown in Fig. 9, the distance between two neighbouring large particles is a function of angle θ . Hence, the distance, $d(\theta)$, can be expressed as

$$d(\theta) = (d_S + d_L) \cos\left(\frac{\theta}{2}\right) = (1+x)d_L \cos\left(\frac{\theta}{2}\right). \quad (B1)$$

Assume the small particle is isotropically stuck to the surface of one large particle, then the probability to have two large

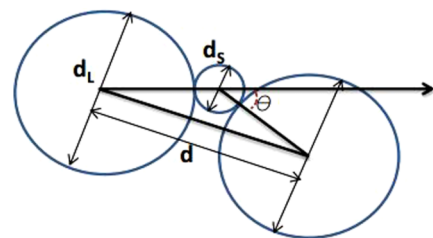


FIG. 9. Configuration for two large particles connected by a small particle.

particles with the angle between θ and $\theta + d\theta$ is proportional to the surface area of small particle accessed by another large particle, that is

$$P(\theta) \propto 2\pi R_S \sin \theta \times R_S d\theta \propto \sin \theta d\theta. \quad (\text{B2})$$

Here, R_S is the radius of small particles.

The geometric arrangement of two large and one small particle also sets the maximum value of θ to satisfy $d(\theta) \geq d_L$. And it turns out to be

$$\cos\left(\frac{\theta_{\max}}{2}\right) = \frac{1}{1+x}. \quad (\text{B3})$$

With the three equations above, the average inter-particle distance can be calculated as an effective ‘‘diameter’’ of one-component SHS system

$$d_L^{\text{eff}} = \frac{\int_0^{\theta_{\max}} d(\theta) P(\theta)}{\int_0^{\theta_{\max}} P(\theta)}$$

and the final result is

$$\frac{d_L^{\text{eff}}}{d_L} = \frac{2}{3} \left(1 + x + \frac{1}{2+x}\right). \quad (\text{B4})$$

The volume fraction of the mapped SHS system is

$$\frac{\phi_L^{\text{eff}}}{\phi_L} = \left(\frac{d_L^{\text{eff}}}{d_L}\right)^3. \quad (\text{B5})$$

The next step is to map out the attraction of the equivalent pure SHS system according to the value of partial structure factor for large particles at $q = 0$, which can be calculated directly from Appendix A. The results are (here, unlike the case in Appendix A, which is for a general multi-component system, ‘‘S’’ and ‘‘L’’ are used to be the subscripts instead of ‘‘1’’ and ‘‘2,’’ respectively):

$$Q_{SS}(0) = 1 + \frac{4\phi_S}{\varepsilon} + \frac{3\phi_S(\phi_S + x\phi_L)}{\varepsilon^2} - \frac{(1+x)^2\phi_S\phi_L}{4\varepsilon} \lambda_{SL},$$

$$Q_{SL}(0) = -\sqrt{\frac{\phi_S\phi_L}{x^3}} \left[\frac{(1+x)^2(1-\phi_S)}{4\varepsilon} \lambda_{SL} - \frac{1+3x}{\varepsilon} - \frac{3(\phi_S + x\phi_L)}{\varepsilon^2} \right],$$

$$Q_{LS}(0) = -\sqrt{x^3\phi_S\phi_L} \left[\frac{(1+1/x)^2(1-\phi_L)}{4\varepsilon} \lambda_{SL} - \frac{1+3/x}{\varepsilon} - \frac{3(\phi_S/x + \phi_L)}{\varepsilon^2} \right],$$

$$Q_{LL}(0) = 1 + \frac{4\phi_L}{\varepsilon} + \frac{3\phi_L(\phi_S/x + \phi_L)}{\varepsilon^2} - \frac{(1+1/x)^2\phi_S\phi_L}{4\varepsilon} \lambda_{SL},$$

$$S_{LL}(0) = (Q^T(0)Q(0))_{LL}^{-1} \\ = \frac{Q_{SS}^2(0) + Q_{LS}^2(0)}{Q_{SS}(0)Q_{LL}(0) - Q_{SL}(0)Q_{LS}(0)}.$$

For the equivalent one-component SHS system with parameters d_L^{eff} , ϕ_L^{eff} , τ_L^{eff} , the structure factor at $q = 0$ is^{36,50}

$$Q^{\text{eff}}(0) = 1 + \phi_L^{\text{eff}} \left[\frac{4 - \phi_L^{\text{eff}}}{(1 - \phi_L^{\text{eff}})^2} - \frac{\lambda}{1 - \phi_L^{\text{eff}}} \right], \\ \lambda = \frac{6}{\phi_L^{\text{eff}}} \left\{ \tau_L^{\text{eff}} + \frac{\phi_L^{\text{eff}}}{1 - \phi_L^{\text{eff}}} - \left[\tau_L^{\text{eff}} + \frac{\phi_L^{\text{eff}}}{1 - \phi_L^{\text{eff}}} \right]^2 \right\}$$

$$- \frac{\phi_L^{\text{eff}}(1 + \phi_L^{\text{eff}}/2)}{3(1 - \phi_L^{\text{eff}})^2} \} 1/2\},$$

$$S^{\text{eff}}(0) = \frac{1}{(Q^{\text{eff}}(0))^2}.$$

The relation between the binary system and the equivalent one-component SHS system is $S^{\text{eff}}(0) = S_{LL}(0)$. Then the mapped attraction τ_L^{eff} is

$$\tau_L^{\text{eff}} = \left[\frac{(1 - \phi_L^{\text{eff}})^2}{36} S_{LL}(0) + \frac{4\phi_L^{\text{eff}} - 1}{18} \sqrt{S_{LL}(0)} - \frac{14(\phi_L^{\text{eff}})^2 - 4\phi_L^{\text{eff}} - 1}{36(1 - \phi_L^{\text{eff}})^2} \right] \left/ \left[\frac{2\phi_L^{\text{eff}} + 1}{3(1 - \phi_L^{\text{eff}})} - \frac{1 - \phi_L^{\text{eff}}}{3} \sqrt{S_{LL}(0)} \right] \right]. \quad (\text{B6})$$

From Eqs. (B4)–(B6), it is straightforward to map the binary system to equivalent one-component SHS system.

- ¹C. Zhao, G. Yuan, and C. C. Han, *Soft Matter* **8**, 7036 (2012).
- ²N. J. Wagner and J. F. Brady, *Phys. Today* **62**(10), 27 (2009).
- ³S. Chen, C. Liao, E. Fratini, P. Baglioni, and F. Mallamace, *Colloids Surf., A* **183-185**, 95 (2001).
- ⁴E. J. Yearley, P. D. Goldfrin, T. Perevozchikova, H. Zhang, P. Falus, L. Porcar, M. Nagao, J. E. Curtis, P. Gawande, R. Taing, I. E. Zarraga, N. J. Wagner, and Y. Liu, *Biophys. J.* **106**, 1763 (2014).
- ⁵O. Velev, E. Kaler, and A. Lenhoff, *Biophys. J.* **75**, 2682 (1998).
- ⁶W. Doster and S. Longeville, *Biophys. J.* **93**, 1360 (2007).
- ⁷J. Hansen and I. McDonald, *Theory of simple liquids*, 2nd ed. (Academic, London, 1986).
- ⁸P. N. Pusey and W. van Meegen, *Nature* **320**, 340 (1986).
- ⁹H. Lowen, T. Palberg, and R. Simon, *Phys. Rev. Lett.* **70**, 1557 (1993).
- ¹⁰G. Nagele, *Phys. Rep.* **272**, 215 (1996).
- ¹¹K. Batchelor, *J. Fluid Mech.* **74**, 1 (1976).
- ¹²D. Rosenbaum, P. C. Zamora, and C. F. Zukoski, *Phys. Rev. Lett.* **76**, 150 (1996).
- ¹³D. Frenkel, *Science* **314**, 768 (2006).
- ¹⁴P. Wolde and D. Frenkel, *Science* **277**, 1975 (1997).
- ¹⁵K. Pham, A. Puertas, J. Bergenholtz, S. Egelhaaf, P. N. Pusey, A. B. Schofield, M. E. Cates, M. Fuchs, and W. C. K. Poon, *Science* **296**, 104 (2002).
- ¹⁶V. J. Anderson and H. N. W. Lekkerkerker, *Nature* **416**, 811 (2002).
- ¹⁷K. Dawson, G. Foffi, M. Fuchs *et al.*, *Phys. Rev. E* **63**, 011401 (2000).
- ¹⁸J. C. Crocker, J. A. Matteo, A. D. Dinsmore, and A. G. Yodh, *Phys. Rev. Lett.* **82**, 4352 (1999).
- ¹⁹P. J. Lu, E. Zaccarelli, F. Ciulla, A. B. Schofield, F. Sciortino, and D. A. Weitz, *Nature* **453**, 499 (2008).
- ²⁰F. Oosawa and S. Asakura, *J. Chem. Phys.* **22**, 1255 (1954).
- ²¹S. Asakura and F. Oosawa, *J. Polym. Sci.* **33**, 183 (1958).
- ²²X. Xing, G. Sun, Z. Li, and T. Ngai, *Langmuir* **28**, 16022 (2012).
- ²³P. N. Pusey, A. D. Pirie, and W. C. K. Poon, *Physica A* **201**, 322 (1993).
- ²⁴S. M. Ilett, A. Orrock, W. C. K. Poon, and P. N. Pusey, *Phys. Rev. E* **51**, 1344 (1995).
- ²⁵G. E. Fernandes, D. J. Beltran-Villegas, and M. A. Bevan, *Langmuir* **24**, 10776 (2008).
- ²⁶G. E. Fernandes, D. J. Beltran-Villegas, and M. A. Bevan, *J. Chem. Phys.* **131**, 134705 (2009).
- ²⁷X. Xing, Z. Li, and T. Ngai, *Macromolecules* **42**, 7271 (2009).
- ²⁸G. Meng, N. Arkus, M. P. Brenner, and V. N. Manoharan, *Science* **327**, 560 (2010).
- ²⁹K. Bayliss, J. S. van Duijneveldt, M. A. Faers, and A. W. P. Vermeer, *Soft Matter* **7**, 10345 (2011).
- ³⁰E. G. M. Pelessers, M. A. C. Stuart, and G. J. Fleer, *J. Chem. Soc., Faraday Trans.* **86**, 1355 (1990).
- ³¹A. A. Louis, E. Allahyarov, H. Löwen, and R. Roth, *Phys. Rev. E* **65**, 061407 (2002).
- ³²N. Gnan, E. Zaccarelli, and F. Sciortino, *J. Chem. Phys.* **137**, 084903 (2012).
- ³³M. E. Leunissen, C. G. Christova, A. P. Hynninen, C. P. Royall, A. I. Campbell, A. Imhof, M. Dijkstra, R. van Roij, and A. van Blaaderen, *Nature* **437**, 235 (2005).

- ³⁴G. I. Guerrero-Garcia, E. Gonzalez-Tovar, and M. O. de la Cruz, *Soft Matter* **6**, 2056 (2010).
- ³⁵F. Zhang, M. W. A. Skoda, R. M. J. Jacobs, S. Zorn, R. A. Martin, C. M. Martin, G. F. Clark, S. Weggler, A. Hildebrandt, O. Kohlbacher, and F. Schreiber, *Phys. Rev. Lett.* **101**, 148101 (2008).
- ³⁶R. J. Baxter, *J. Chem. Phys.* **49**, 2770 (1968).
- ³⁷R. J. Baxter, *Aust. J. Phys.* **21**, 563 (1968).
- ³⁸E. Zaccarelli, G. Foffi, P. Tartaglia, F. Sciortino, and K. A. Dawson, *Prog. Colloid Polym. Sci.* **115**, 371 (2000).
- ³⁹B. Barboy and R. Tenne, *Chem. Phys.* **38**, 369 (1979).
- ⁴⁰M. H. G. M. Penders and A. Vrij, *Physica A* **173**, 532 (1991).
- ⁴¹R. Fantoni, D. Gazzillo, and A. Giacometti, *J. Chem. Phys.* **122**, 034901 (2005).
- ⁴²R. Fantoni, D. Gazzillo, and A. Giacometti, *Phys. Rev. E* **72**, 011503 (2005).
- ⁴³D. Gazzillo and A. Giacometti, *J. Chem. Phys.* **113**, 9837 (2000).
- ⁴⁴D. Gazzillo and A. Giacometti, *J. Chem. Phys.* **120**, 4742 (2004).
- ⁴⁵E. Dickinson, *J. Colloid Interface Sci.* **132**, 274 (1989).
- ⁴⁶E. Dickinson, *J. Chem. Soc., Faraday Trans.* **86**, 439 (1990).
- ⁴⁷E. Dickinson and L. Eriksson, *Adv. Colloid Interface Sci.* **34**, 1 (1991).
- ⁴⁸E. Dickinson, *J. Chem. Soc., Faraday Trans.* **91**, 4413 (1995).
- ⁴⁹R. J. Baxter, *J. Chem. Phys.* **52**, 4559 (1970).
- ⁵⁰R. O. Watts, D. Henderson, and R. J. Baxter, *Adv. Chem. Phys.* **21**, 421 (1971).
- ⁵¹M. A. Miller and D. Frenkel, *Phys. Rev. Lett.* **90**, 135702 (2003).
- ⁵²M. A. Miller and D. Frenkel, *J. Chem. Phys.* **121**, 535 (2004).
- ⁵³H. Verduin and J. K. G. Dhont, *J. Colloid Interface Sci.* **172**, 425 (1995).
- ⁵⁴B. Barboy, *J. Chem. Phys.* **61**, 3194 (1974).
- ⁵⁵J. C. Chiew and E. D. Glandt, *J. Phys. A: Math. Gen.* **16**, 2599 (1983).
- ⁵⁶B. Barboy, *Chem. Phys.* **11**, 357 (1975).
- ⁵⁷C. Robertus, W. H. Philipse, J. G. H. Joosten, and Y. K. Levine, *J. Chem. Phys.* **90**, 4482 (1989).
- ⁵⁸J. W. Perram and E. R. Smith, *Chem. Phys. Lett.* **35**, 138 (1975).
- ⁵⁹J. W. Perram and E. R. Smith, *Proc. R. Soc. London, Ser. A* **353**, 193 (1977).
- ⁶⁰W. G. T. Kranendonk and D. Frenkel, *Mol. Phys.* **64**, 403 (1988).
- ⁶¹M. A. Miller and D. Frenkel, *J. Phys.: Condens. Matter* **16**, s4901 (2004).
- ⁶²C. Regnaut and J. C. Ravey, *J. Chem. Phys.* **91**, 1211 (1989).
- ⁶³S. V. G. Menon, C. Manohar, and K. S. Rao, *J. Chem. Phys.* **95**, 9186 (1991).
- ⁶⁴G. Stell, *J. Stat. Phys.* **63**, 1203 (1991).
- ⁶⁵G. Foffi, E. Zaccarelli, F. Sciortino, P. Tartaglia, and K. A. Dawson, *J. Stat. Phys.* **100**, 363 (2000).
- ⁶⁶C. Zhao, G. Yuan, and C. C. Han, *Macromolecules* **45**, 9468 (2012).
- ⁶⁷M. Dijkstra, R. van Roij, and R. Evans, *Phys. Rev. E* **59**, 5744 (1999).
- ⁶⁸See supplementary material at <http://dx.doi.org/10.1063/1.4913197> for the calculation of the accepted region of the mapping method, the structure factor comparison along the EHS line, and the phase diagrams plotted in different scales.
- ⁶⁹R. H. Smellie, Jr. and V. K. L. Mer, *J. Colloid Sci.* **23**, 589 (1958).
- ⁷⁰U. Bengtzelius, W. Gotze, and A. Sjolander, *J. Phys. C: Solid State Phys.* **17**, 5915 (1984).
- ⁷¹W. Gotze and L. Sjogren, *Rep. Prog. Phys.* **55**, 241 (1992).
- ⁷²L. Yeomans-Reyna and M. Medina-Noyola, *Phys. Rev. E* **64**, 066114 (2001).
- ⁷³R. Juarez-Maldonado, M. A. Chavez-Rojo, P. E. Ramirez-Gonzalez, L. Yeomans-Reyna, and M. Medina-Noyola, *Phys. Rev. E* **76**, 062502 (2007).
- ⁷⁴J. Bergenholtz, A. A. Romagnoli, and N. J. Wagner, *Langmuir* **11**, 1559 (1995).